arXiv:1611.07949v1 [nucl-th] 23 Nov 2016

Structure of ^{14}C and ^{14}O nuclei within a five-cluster model

B. E. Grinyuk and D. V. Piatnytskyi

Bogolyubov Institute for Theoretical Physics,
National Academy of Sciences of Ukraine,
Metrolohichna 14-b, UA-03143 Kyiv, Ukraine

(Dated: November 24, 2016)

Within a five-particle model (three α-particles plus two nucleons), the structure functions of mirror nuclei ^{14}C and ^{14}O are studied. Using the variational approach with Gaussian bases, the energies and wave functions are calculated for these five-particle systems. Two spatial configurations in the ground-state wave function are revealed. The r.m.s. charge radius of ^{14}O nucleus is found to be 2.415 ± 0.005 fm. The charge density distributions and the form factors of both nuclei are predicted. The pair correlation functions are analyzed, and the r.m.s. relative distances are calculated. The momentum distributions of particles are found.

PACS numbers: 27.20.+n, 1.60.Gx, 21.10.Ft, 21.10.Gv
Keywords: Cluster structure of ^{14}C and ^{14}O nuclei, r.m.s. charge radii, charge density distributions, form factors, pair correlation functions, momentum distributions

I. INTRODUCTION

Radioactive mirror nuclei ^{14}C and ^{14}O in the ground state are very similar by their structures, a small difference being produced by an additional Coulomb repulsion in ^{14}O nucleus as compared to ^{14}C one. This fact can be used to determine the radius of the very rare isotope ^{14}O not yet measured experimentally. The idea is to treat both nuclei within one approach under the condition that the experimental radius of ^{14}C is well fitted, as well as the experimental binding energies of these nuclei. The contribution of the additional Coulomb repulsion can be taken into account accurately, and thus the radius of ^{14}O nucleus can be obtained.

In the present paper, we consider the mirror nuclei ^{14}C and ^{14}O as composed from three α-particles and two extra nucleons (neutrons in ^{14}C nucleus and protons in ^{14}O one). Such model [1] may have a rather good accuracy as it was shown by calculations of the structure functions of three- and four-cluster nuclei [2–6] consisting of α-particles and two extra nucleons. For the ground state of both nuclei and some low-lying energy levels (for which the excitation of an α-particle can be neglected), our five-particle model can be competitive in accuracy with the approaches like [7], where one has to deal with all the nucleon degrees of freedom. To solve the five-particle problem, we exploit the variational method with Gaussian bases [8, 9] widely used to study the bound states of few-particle systems.

In the next section, the formulation of the Hamiltonian is given. The radii of both nuclei and density distributions are discussed in section 3. In sections 4, 5, and 7, we present the rest main structure functions of ^{14}C and ^{14}O nuclei (elastic charge form factors, pair correlation functions, and the momentum distributions of α-particles and extra nucleons). In section 6, we study the characteristic features of the ground-state wave functions of both nuclei, where two spatial configurations are revealed.

II. STATEMENT OF THE PROBLEM

Within our five-particle model, the Hamiltonian for ^{14}O nucleus is assumed to have the form:

$$\hat{H} = \sum_{i=1}^{2} \frac{\mathbf{p}_i^2}{2m_p} + \sum_{i=3}^{5} \frac{\mathbf{p}_i^2}{2m_\alpha} + U_{pp}(r_{12}) + \sum_{j>i=3}^{5} \hat{U}_{\alpha\alpha}(r_{ij}) +$$

$$+ \sum_{i=1}^{2}\sum_{j=3}^{5} \hat{U}_{p\alpha}(r_{ij}) + \sum_{j>i=1}^{5} \frac{Z_i Z_j e^2}{r_{ij}}, \tag{1}$$

where indices p and α denote a proton and an α-particle, respectively. In (1), $Z_1 = Z_2 = 1$ are the charges of protons (in units of elementary charge e), and $Z_3 = Z_4 = Z_5 = 2$ are the charges of α-particles (in the same units).

Within our model, the Hamiltonian for ^{14}C nucleus is very similar to (1), but with $Z_1 = Z_2 = 0$, since the neutrons have zero charge. We assume the potentials $\hat{U}_{\alpha\alpha}$ are the same for both nuclei, as well as the interaction potential between the extra neutrons U_{nn} coincides with U_{pp} due to the charge independence of nuclear forces. As for the potentials $\hat{U}_{p\alpha}$ in the case of ^{14}O nucleus and $\hat{U}_{n\alpha}$ in the case of ^{14}C one, their parameters may be slightly different, because the density distributions of protons and neutrons inside the α-particle are not identical mainly due to the Coulomb repulsion between protons. We note that the local potential U_{nn} in the singlet state was successfully used in studying the structure of ^{6}He [4] and ^{10}Be [6] nuclei. The potentials $U_{n\alpha}$ and $U_{p\alpha}$, as well as the interaction potential between α-particles $U_{\alpha\alpha}$, are of a generalized type with local and non-local (separable) terms. This type of potentials was first proposed [10, 11] to simulate the exchange effects between particles in interacting clusters and was successfully used, in particular, in calculations [2, 4, 6] of multicluster nuclei. The parameters of the interaction potentials used in this work are given in [1], and the calculations within our model with these potentials result in the experimental binding energies of both nuclei under consideration, as well as the experimental charge radius of ^{14}C nucleus.

The ground-state energy and the wave function are calculated with the use of variational method in the Gaussian representation [8, 9], which proved its high accuracy in calculations of few-particle systems. For the ground $J^\pi = 0^+$ state, the wave function can be expressed in the form

$$\Phi = \hat{S}\sum_{k=1}^{K} C_k \varphi_k \equiv \hat{S}\sum_{k=1}^{K} C_k \; exp\left(-\sum_{j>i=1}^{5} a_{k,ij}(\mathbf{r}_i - \mathbf{r}_j)^2\right), \tag{2}$$

where $\hat{S}$ is the symmetrization operator, and the linear coefficients C_k and nonlinear parameters $a_{k,ij}$ are variational parameters. The greater the dimension K of the basis, the more accurate the result can be obtained. The linear coefficiens can be found within the Galerkin method from the system of linear equations determining the energy of the system:

$$\sum_{m=1}^{K} C_m \left\langle \hat{S}\varphi_k \left| \hat{H} - E \right| \hat{S}\varphi_m \right\rangle = 0, \quad k = 0, 1, ..., K. \tag{3}$$

The matrix elements in (3) are known to have explicit form for potentials like the Coulomb potential or the ones having a Gaussian expansion. Our potentials [1] between particles just have the form of a few Gaussian functions, including the Gaussian form factor in the separable repulsive term. Thus, system (3) becomes a system of algebraic equations. We achieved the necessary high accuracy, by using up to $K = 400$ functions of the Gaussian basis. To fix the non-linear variational parameters

Table I: Calculated energies (MeV) (subtracting the own energies of α-particles), r.m.s. relative distances, and r.m.s. radii (fm) for ^{14}C and ^{14}O nuclei

Nucleus	E	r_{NN}	$r_{N\alpha}$	$r_{\alpha\alpha}$	R_N	R_α	R_m	$R_{\rm ch}$
^{14}C	−20.398	2.621	2.667	3.189	1.786	1.852	2.433	2.500
^{14}O	−13.845	2.732	2.750	3.239	1.864	1.882	2.461	2.415

$a_{k,ij}$, we used both the stochastic approach [8, 9] and regular variational methods. This enables us to obtain the best accuracy at reasonable values of the dimension K.

As a result, we have the wave functions of the ground state for both nuclei under consideration within the five-particle model. This enables us to analyze the structure functions of ^{14}C and ^{14}O nuclei. In the next section, the charge density distributions and charge r.m.s. radii are discussed.

III. DENSITY DISTRIBUTIONS AND RADII OF ^{14}C AND ^{14}O NUCLEI

The probability density distribution $n_i(r)$ of the i-th particle in a system of particles with the wave function $|\Phi\rangle$ is known to be

$$n_i(r) = \langle\Phi|\,\delta\left(\mathbf{r} - (\mathbf{r}_i - \mathbf{R}_{\rm c.m.})\right)|\Phi\rangle\,, \tag{4}$$

where $\mathbf{R}_{\rm c.m.}$ is the center of mass of the system. The probability density distributions are normalized as $\int n_i(r)\,d\mathbf{r} = 1$.

In Fig. 1, we depict the values $r^2 n_p(r)$ and $r^2 n_\alpha(r)$, respectively, for the density distributions of extra protons and α-particles in ^{14}O nucleus. The profiles very close to those shown in Fig. 1 were obtained for ^{14}C nucleus in [1]. It is clearly seen that extra nucleons in both nuclei move mainly inside the ^{12}C cluster formed by α-particles. At the same time, the secondary maximum of curve 1 at $r \approx 3.4$ fm means that the extra protons in ^{14}O nucleus can be found off the ^{12}C cluster (with a probability $\simeq 0.16$). Similarly, the extra neutrons in ^{14}C nucleus can be found off the ^{12}C cluster (with a probability $\simeq 0.14$). Two above-mentioned maxima on curve 1 are the consequence of two configurations distinctly present in the nuclei under consideration (see below).

To find the r.m.s. radius R_i of the density distribution $n_i(r)$, one has to calculate the integral $R_i = \left(\int r^2 n_i(r)\,d\mathbf{r}\right)^{1/2}$. In Table 1, the main calculated parameters are given for both nuclei. In particular, the r.m.s. radii R_n and R_α obtained for "pointlike" extra neutrons and α-particles in ^{14}C nucleus are seen to be less than the corresponding r.m.s. radii R_p and R_α for ^{14}O system. This is explained by the additional Coulomb repulsion in ^{14}O nucleus due to the presence of extra protons instead of extra neutrons present in ^{14}C. As a result, the r.m.s. radius of the mass distribution R_m in ^{14}O is also larger than R_m for ^{14}C. At the same time, we have $R_N < R_\alpha$ for both nuclei (where $R_N \equiv R_n$ for ^{14}C and $R_N \equiv R_p$ for ^{14}O). This inequality is directly related to the fact that the extra nucleons are settled mainly inside the ^{12}C cluster (see Fig. 1).

To find the charge density distributions of the nuclei with regard for finite sizes of α-particles and extra protons, we use the Helm approximation [12, 13]. Within this approach, the charge density distribution for ^{14}C nucleus,

$$n_{\rm ch}(r) = \int n_\alpha\left(\left|\mathbf{r} - \mathbf{r}'\right|\right) n_{\rm ch,^4He}\left(r'\right) d\mathbf{r}', \tag{5}$$

is a convolution product of the density distribution n_α for the probability to find an α-particle inside the ^{14}C nucleus with the charge density distribution $n_{\rm ch,^4He}$ of an α-particle itself. The value of n_α is calculated within our five-particle model, while $n_{\rm ch,^4He}$ follows from the experimental form

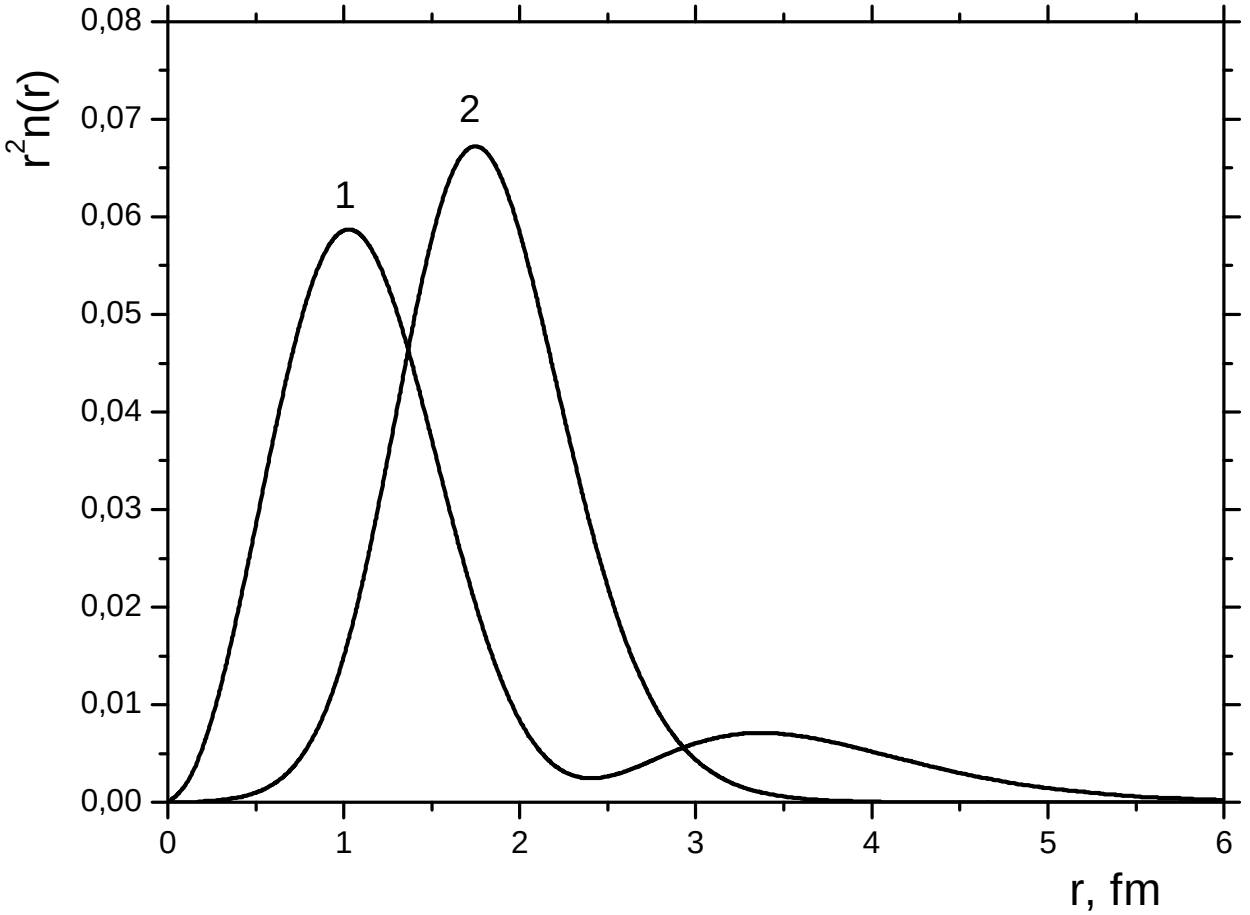

Figure 1: Probability density distributions multiplied by r^2 obtained for extra protons (curve 1) and α-particles (curve 2) in ^{14}O nucleus

factor [14]. In relation (5), we neglect the small contribution of extra neutrons. We normalize the charge density distribution as $\int n_{\rm ch}\left(r\right) d\mathbf{r} = 1$, i.e. one has to multiply it by Ze to obtain the necessary dimensional units.

In case of ^{14}O nucleus, instead of (5), we have two following terms in the expression for $n_{\rm ch}\left(r\right)$ due to the role of extra protons:

$$n_{\rm ch}\left(r\right) = \frac{3}{4}\int n_{\alpha}\left(\left|\mathbf{r}-\mathbf{r}'\right|\right) n_{{\rm ch},^4{\rm He}}\left(r'\right) d\mathbf{r}' + \frac{1}{4}\int n_{p}\left(\left|\mathbf{r}-\mathbf{r}'\right|\right) n_{{\rm ch},p}\left(r'\right) d\mathbf{r}' \qquad (6)$$

(the coefficients 3/4 and 1/4 are proportional to the charges of three α-particles and two extra protons, respectively).

The charge density distributions for ^{14}C and ^{14}O nuclei are shown in Fig. 2. For comparison, the dashed line presents the density distribution of the probability to find an α-particle in ^{14}C nucleus (almost the same distribution could be shown for ^{14}O). We distinctly see a dip near the origin in the probability density distribution of "poinlike" α-particles, but the integration in the convolution product (5), i.e., the account for a finite size of α-particles, results in the maximum of the charge density distribution of ^{14}C nucleus near $r = 0$, nothing to say about ^{14}O nucleus, where the contribution of charged extra protons in (6) makes the maximum at $r = 0$ even more pronounced. Since the distributions are normalized to 1, the charge density distribution of ^{14}O nucleus should be lower than that of ^{14}C one at larger distances important for the calculation of

the r.m.s. charge radii. As a result, we have the inequality:

$$R^2_{\mathrm{ch},^{14}\mathrm{O}} \equiv \int r^2 n_{\mathrm{ch},^{14}\mathrm{O}}(r)\, d\mathbf{r} < R^2_{\mathrm{ch},^{14}\mathrm{C}} \equiv \int r^2 n_{\mathrm{ch},^{14}\mathrm{C}}(r)\, d\mathbf{r}. \tag{7}$$

Within the Helm approximation for the density distributions (5) and (6), the charge radii squared are known to be

$$R^2_{\mathrm{ch},^{14}\mathrm{C}} = R^2_{\alpha,^{14}\mathrm{C}} + R^2_{\mathrm{ch},^{4}\mathrm{He}}, \tag{8}$$

$$R^2_{\mathrm{ch},^{14}\mathrm{O}} = \frac{3}{4}\left(R^2_{\alpha,^{14}\mathrm{O}} + R^2_{\mathrm{ch},^{4}\mathrm{He}}\right) + \frac{1}{4}\left(R^2_{\mathrm{p},^{14}\mathrm{O}} + R^2_{\mathrm{ch,p}}\right). \tag{9}$$

Due to the fact that $R_{\mathrm{p},^{14}\mathrm{O}} < R_{\alpha,^{14}\mathrm{O}}$, i.e. the extra protons move (on the average) closer to the center of ^{14}O nucleus than the α-particles do (see Table 1), and due to the well-known experimental fact that $R_{\mathrm{ch,p}} < R_{\mathrm{ch},^{4}\mathrm{He}}$, we again confirm inequality (III). The calculated r.m.s. charge radii are given in Table 1. Since the errors of the experimental radius of an α-particle [15, 16] are of the order of ± 0.003 fm, we estimate the accuracy of our result for the charge r.m.s. radius of ^{14}O to be of the order of ± 0.005 fm. We hope for that the future experiments should confirm the calculated r.m.s. charge radius of ^{14}O nucleus: $R_{\mathrm{ch},^{14}\mathrm{O}} = 2.415 \pm 0.005$ fm.

It is obvious that the mass r.m.s. radius of ^{14}O nucleus is, vice versa, greater than that of ^{14}C nucleus (see Table 1), because both nuclei have very similar mass distribution structures, and ^{14}O nucleus has the lower binding energy and larger relative distances between particles due to the additional Coulomb repulsion of extra protons.

IV. ELASTIC CHARGE FORM FACTORS OF ^{14}C AND ^{14}O NUCLEI

The elastic charge form factor $F_{\mathrm{ch}}(q)$ can be found by a Fourier transformation of the density distribution $n_{\mathrm{ch}}(r)$,

$$F_{\mathrm{ch}}(q) = \int \exp\left(-i\left(\mathbf{qr}\right)\right) n_{\mathrm{ch}}(r)\, d\mathbf{r}. \tag{10}$$

In the Helm approximation for $n_{\mathrm{ch}}(r)$ of ^{14}C nucleus, the convolution product (5) for the charge density distribution transforms to a product, and for the charge form factor of ^{14}C one has

$$F_{\mathrm{ch},^{14}\mathrm{C}}(q) = F_{\alpha,^{14}\mathrm{C}}(q)\, F_{\mathrm{ch},^{4}\mathrm{He}}(q), \tag{11}$$

where $F_{\alpha,^{14}\mathrm{C}}(q)$ is the Fourier transform of the probability density distribution of α-particles in ^{14}C nucleus, and $F_{\mathrm{ch},^{4}\mathrm{He}}(q)$ is the form factor of ^{4}He. The profile of $F_{\alpha,^{14}\mathrm{C}}(q)$ is calculated within our five-particle model, and the form factor of ^{4}He nucleus is taken from the experiment [14].

It is clear from expression (11) that the elastic charge form factor of ^{14}C nucleus should become zero at that momentum transfer squared q^2, where any of two multipliers in (11) becomes zero. The absolute value of the form factor at corresponding values of q^2 should have "dips". In Fig. 3, we depict the absolute value of the elastic charge form factor (11) (solid line) together with both multipliers from the right-hand side of relation (11) (dashed lines). The dip at $q^2 \simeq 10$ fm^{-2} is intrinsic to ^{4}He nucleus [14], and it reveals itself in all the form factors of light nuclei obtained within the α-particles plus some neutrons model (see, e.g., form factors of ^{6}He [4] or ^{10}Be [6]). The dip at $q^2 \simeq 3.7$ fm^{-2} is proper to the form factor $F_{\alpha,^{14}\mathrm{C}}(q)$ in (11). Since its properties are determined by three α-particles forming the ^{12}C cluster inside the ^{14}C nucleus, it is not surprising that we observe the first dip for the form factor of ^{12}C nucleus [17, 18] at almost the same $q^2 \simeq 3.4$

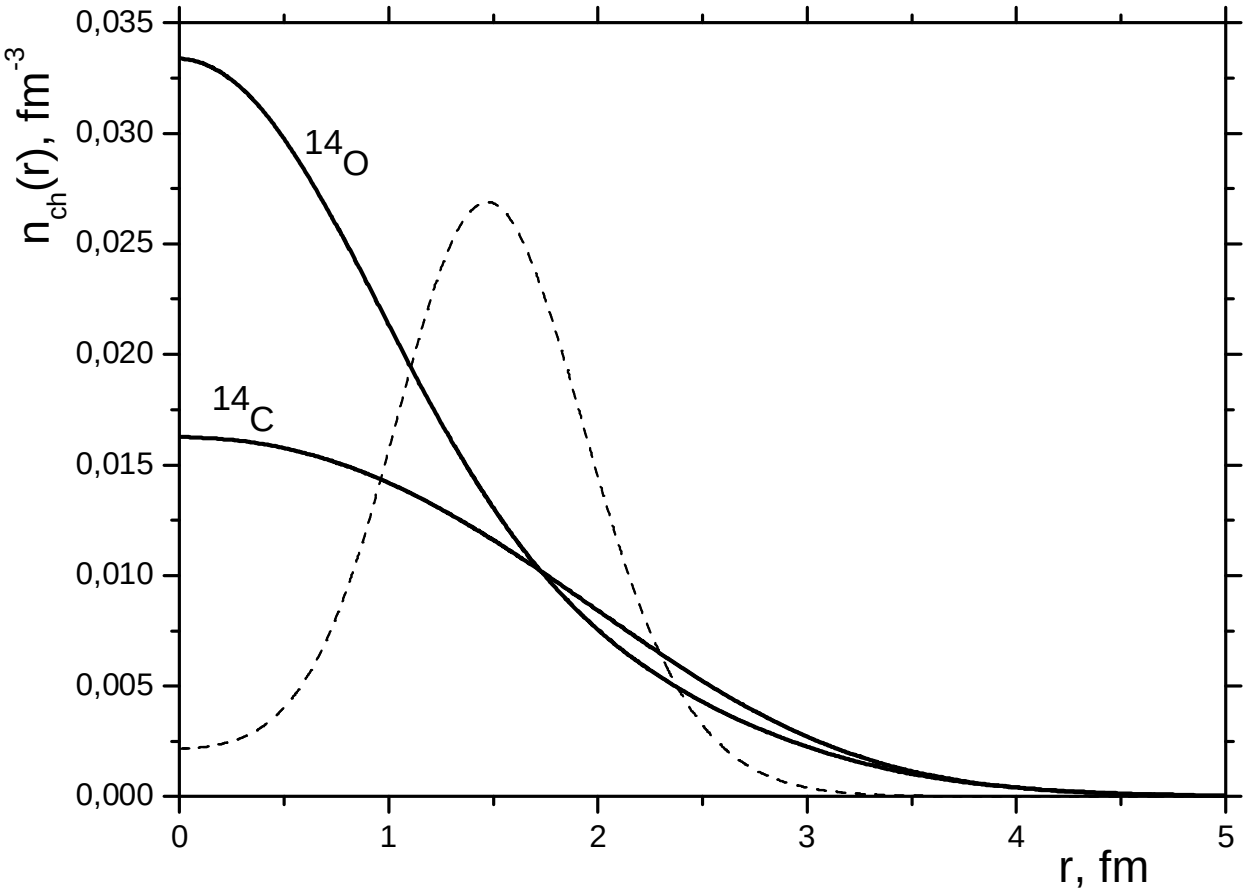

Figure 2: Charge density distributions in ^{14}C and ^{14}O nuclei (normalized as $\int n_{ch}(r)\, d\mathbf{r} = 1$). The dashed line depicts the probability density distribution of α-particles in ^{14}C nucleus

fm^{-2}. This means that the ^{12}C cluster in ^{14}C nucleus is only slightly disturbed by two extra neutrons, and just this cluster is responsible for the first dip in the elastic charge form factor of ^{14}C nucleus.

Passing to the charge form factor of ^{14}O nucleus, we should consider the contribution of extra protons to the charge density distribution (6) of this system. As a result, the elastic form factor, i.e. the Fourier transform of the charge density distribution (6), contains two terms:

$$F_{\mathrm{ch},^{14}\mathrm{O}}(q) = \frac{3}{4} F_{\alpha,^{14}\mathrm{O}}(q)\, F_{\mathrm{ch},^{4}\mathrm{He}}(q) + \frac{1}{4} F_{p,^{14}\mathrm{O}}(q)\, F_{\mathrm{ch},p}(q)\,, \tag{12}$$

where $F_{p,^{14}\mathrm{O}}(q)$ is a Fourier transform of the probability density distribution of extra protons in ^{14}O nucleus, and $F_{\mathrm{ch},p}(q)$ is the charge form factor of the proton itself [19]. The rest notations are similar to ones in formula (11). Although the first term on the right-hand side of (12) is very similar to expression (11) and becomes zero at the same momentum transfer squared q^2 as the form factor (11) does, the second term in (12) (present due the extra protons) is a smoothly decreasing function. Thus, the total expression does not become zero, though the first term does. In Fig. 4, the absolute value of the elastic charge form factor of ^{14}O nucleus is shown (solid line 1). In the contrary to the form factor of ^{14}C nucleus (Fig. 3), it has no dips within the presented range of q^2. The dashed lines show the calculated $F_{p,^{14}\mathrm{O}}(q)$ (dashed line 2) and the experimental form factor $F_{\mathrm{ch},p}(q)$ [19] (dashed line 3).

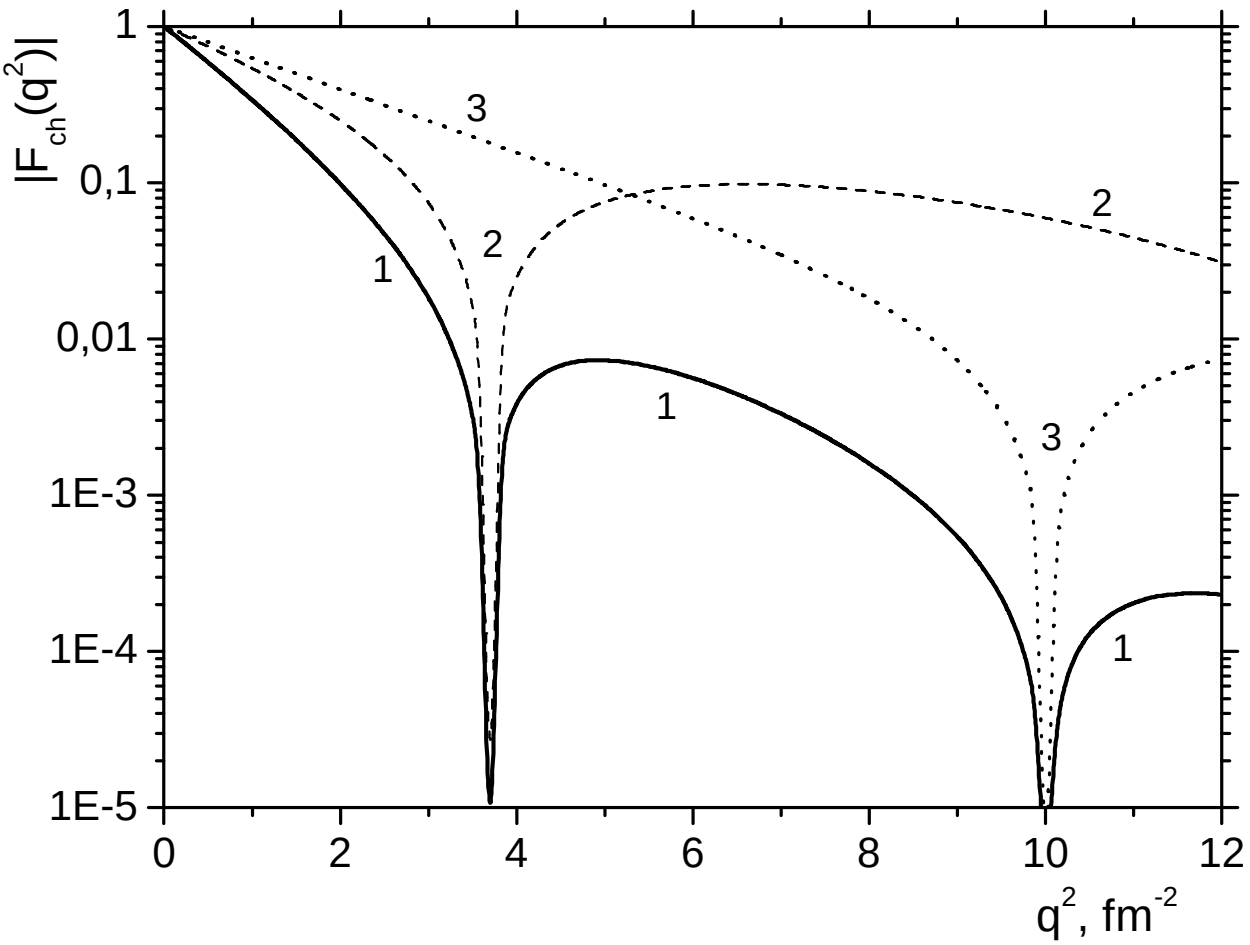

Figure 3: Elastic charge form factor of ^{14}C nucleus (solid line 1). Dashed line 2 depicts the calculated form factor $F_{\alpha,^{14}\mathrm{C}}(q)$, and dashed line 3 depicts the experimental form factor [14] of ^{4}He nucleus

V. PAIR CORRELATION FUNCTIONS AND RELATIVE DISTANCES

More information about the structures of ^{14}C and ^{14}O nuclei can be obtained from the analysis of the pair correlation functions. The pair correlation function $g_{ij}(r)$ for a pair of particles i and j can be defined as follows:

$$g_{ij}(r) = \langle \Phi | \, \delta(\mathbf{r} - (\mathbf{r}_i - \mathbf{r}_j)) \, | \Phi \rangle , \tag{13}$$

and it is known to be the density of the probability to find the particles i and j at a definite distance r. The r.m.s. relative distances squared $\left\langle r_{ij}^2 \right\rangle$ are directly expressed through the pair correlation functions g_{ij}:

$$\left\langle r_{ij}^2 \right\rangle = \int r^2 g_{ij}(r) \, d\mathbf{r}. \tag{14}$$

The calculated r.m.s. relative distances between particles are given in Table 1 for ^{14}C and ^{14}O nuclei. As was mentioned above, due to the additional Coulomb repulsion in ^{14}O as compared to ^{14}C nucleus, all the corresponding relative distances in ^{14}O nucleus are greater than those in ^{14}C.

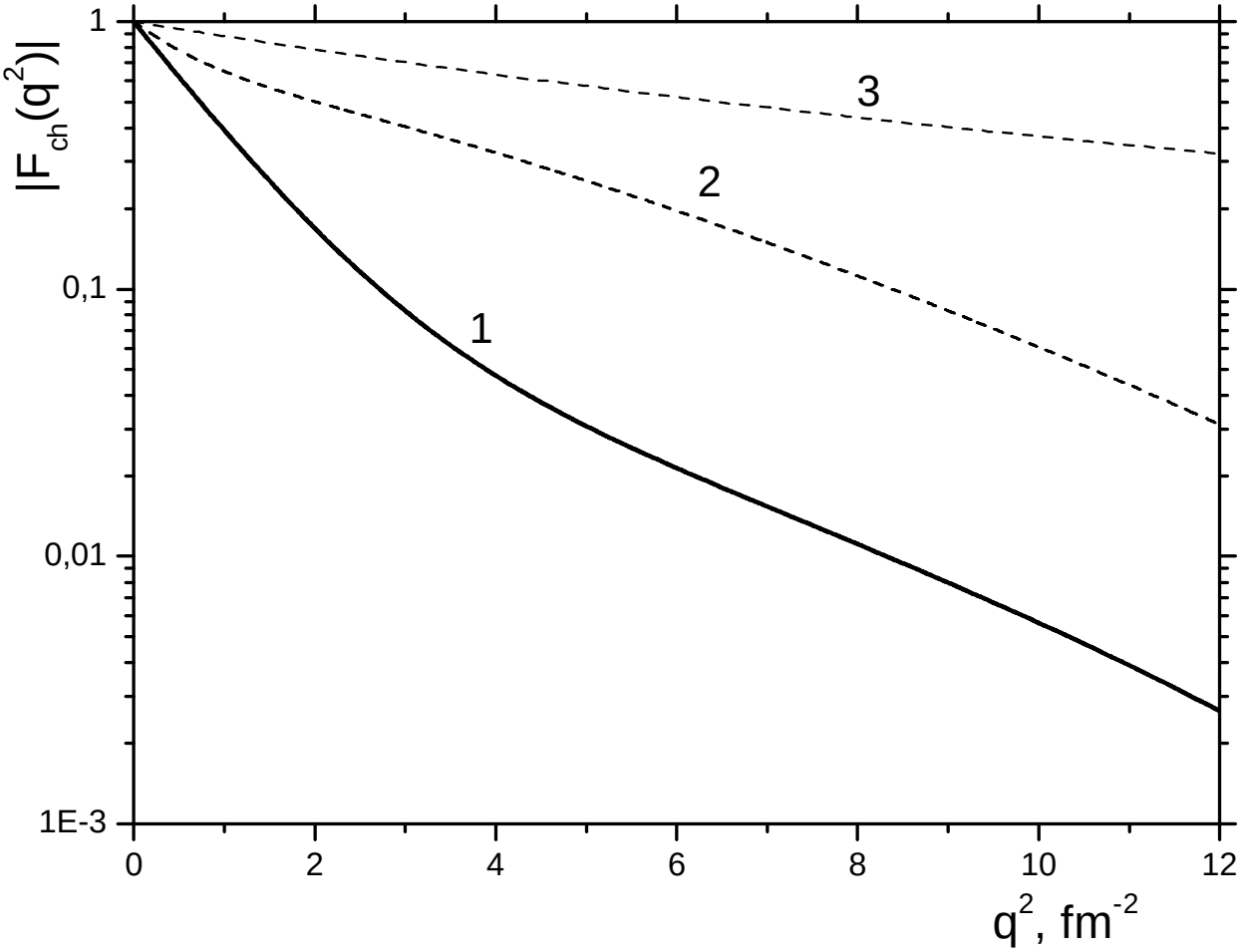

Figure 4: Elastic charge form factor of ^{14}O nucleus (solid line 1). Dashed lines 2 and 3 present the calculated form factor $F_{\mathrm{p},^{14}\mathrm{O}}(q)$ and experimental form factor $F_{\mathrm{ch},p}(q)$ of a proton [19], respectively

We note that the r.m.s. radii R_i are connected with the r.m.s. relative distances r_{jk}:

$$R_i^2 = \frac{1}{M^2}\left((M-m_i)\sum_{j\neq i} m_j r_{ij}^2 \;\; - \sum_{j<k\,(j\neq i,k\neq i)} m_j m_k r_{jk}^2\right), \tag{15}$$

where M is the total mass of the system of particles. Thus, the r.m.s. radii could be calculated with the use of the pair correlation functions and relations (14) and (15).

Since the average of a pairwise local potential $V_{ij}(r)$ is expressible directly through the pair correlation function $g_{ij}(r)$,

$$\langle\Phi|\, V_{ij}\,|\Phi\rangle = \int V_{ij}(r)\, g_{ij}(r)\, d\mathbf{r}, \tag{16}$$

the variational principle makes the profile of $g_{ij}(r)$ such that it has a maximum, where the potential is attractive, and a minimum in the area of repulsion (if the role of the kinetic energy is not crucial). The α-particles have about four times greater mass than extra nucleons, and thus their kinetic energy is essentially smaller than that of nucleons (see below). As a result, the pair correlation function $g_{\alpha\alpha}(r)$ profile is determined mainly by the potential $\hat{U}_{\alpha\alpha}$ and has a pronounced maximum (curve 1 in Fig. 5) near the minimum of the potential attraction. On the other hand, due to the

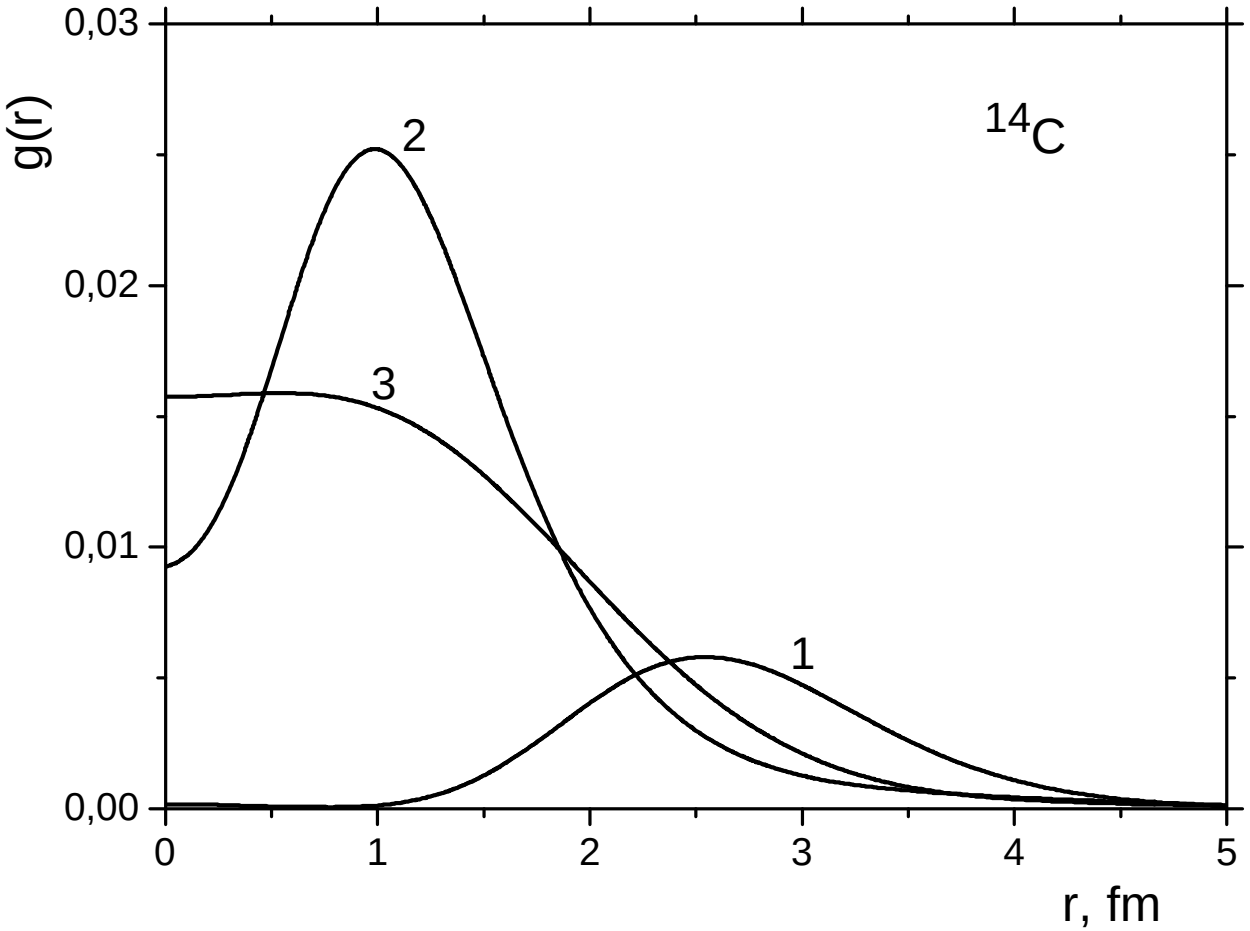

Figure 5: Pair correlation functions for ^{14}C nucleus: $g_{\alpha\alpha}(r)$ - curve 1, $g_{nn}(r)$ - curve 2, and $g_{n\alpha}(r)$ - curve 3

presence of a local repulsion in the same potential near the origin, the profile of $g_{\alpha\alpha}(r)$ has a dip at short distances. Thus, the profile of $g_{\alpha\alpha}(r)$ shows that α-particles are mainly settled at a definite distances $r_{\alpha\alpha}$ (see Table 1) and form a triangle of ^{12}C cluster.

The extra nucleon pair correlation function ($g_{nn}(r)$ for ^{14}C, as well as $g_{pp}(r)$ for ^{14}O), also has a dip at short distances (see Fig. 5, curve 2) due to the presence of a short-range repulsion in our singlet nucleon-nucleon potential [1, 4, 6]. The function $g_{n\alpha}(r)$ has no pronounced dip in the origin, since our model [1] of generalized potential between a nucleon and an α-particle contains the local pure attractive potential plus the non-local (separable) repulsion of greater radius.

VI. TWO CONFIGURATIONS IN ^{14}C AND ^{14}O NUCLEI

To make the structure of the ground state of ^{14}C and ^{14}O nuclei more clear, let us consider the quantity $P(r,\rho,\theta)$ proportional to the density of the probability to find extra nucleons at a definite relative distance r and to find their center of mass at a distance ρ from the center of mass of ^{12}C cluster:

$$P(r,\rho,\theta) = r^2\rho^2 \left\langle \Phi \right| \delta\left(\mathbf{r}-\mathbf{r}_{NN}\right) \delta\left(\boldsymbol{\rho}-\boldsymbol{\rho}_{(NN),(3\alpha)}\right) \left|\Phi\right\rangle, \tag{17}$$

where θ is the angle between the vectors $\mathbf{r}$ and $\boldsymbol{\rho}$. The value $P(r,\rho,\theta)$ is depicted in Fig. 6 for $\theta = 0^\circ$, $\theta = 30^\circ$, $\theta = 45^\circ$, and $\theta = 90^\circ$ as a function of r and ρ. Two peaks on the $P(r,\rho,\theta)$ surface

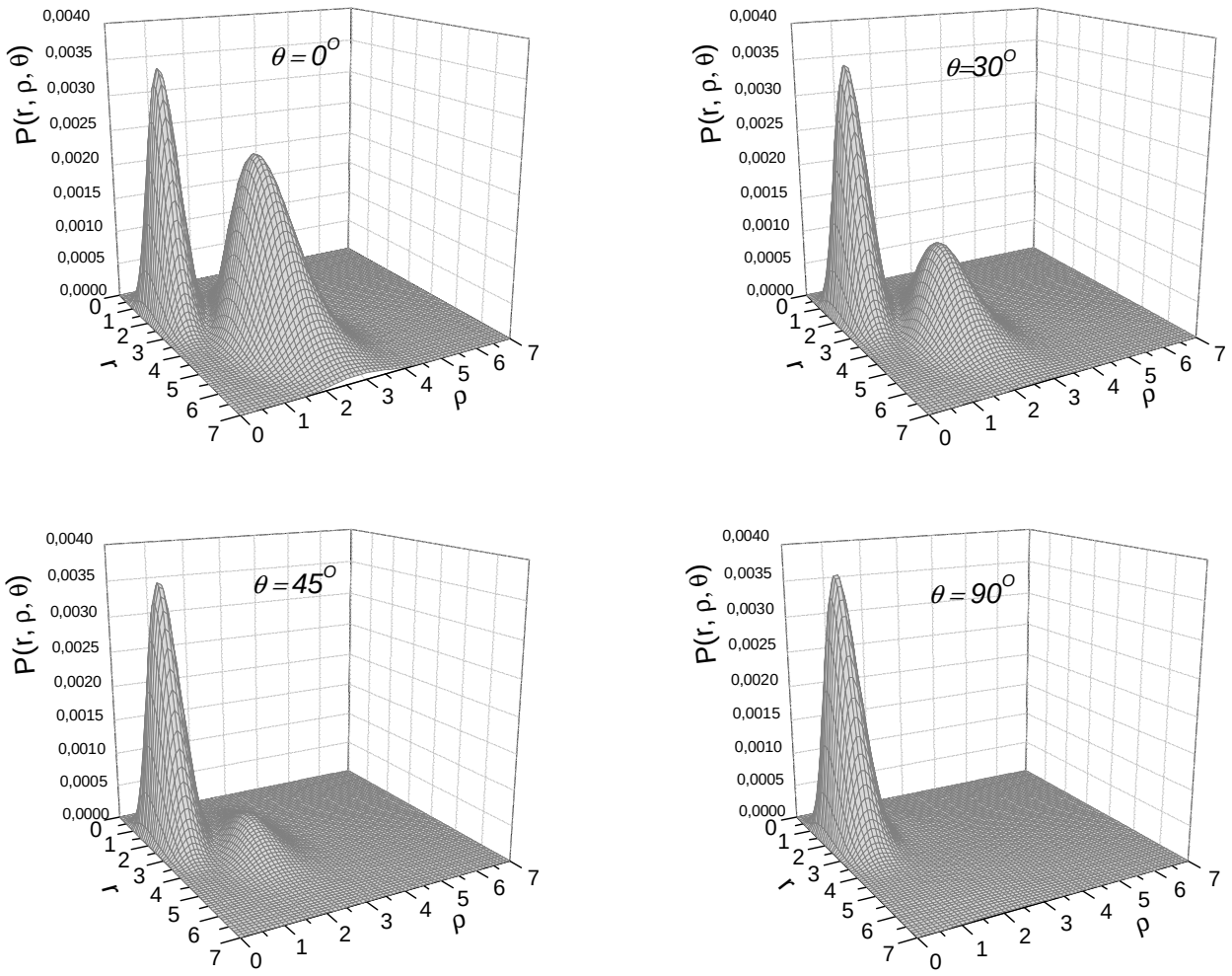

Figure 6: Two configurations in the ground state of ^{14}C nucleus manifesting themselves in the $P(r, \rho, \theta)$ function at different angles θ

are observed at $\theta = 0°$, and only one peak at $\theta = 90°$. The rest angles give intermediate results (see Fig. 6 for $\theta = 30°$ and $\theta = 45°$). If it were not the multiplier $r^2\rho^2$ in (17), the main peak present at all the angles θ would be settled just at $\rho = 0$, i.e. the center of mass of ^{12}C cluster and that of the dinucleon one would coincide. The second peak reveals itself mainly at $\theta = 0°$, and it corresponds to a configuration, where the dinucleon subsystem touches the center of ^{12}C cluster by one of the extra nucleons, and another one is comparatively far from the center of the nucleus (it is out of ^{12}C cluster). Just this configuration makes a contribution to the second maximum of the extra nucleon probability density distribution (see Fig. 1). In this configuration, the center of mass of the subsystem of extra nucleons does not coincide with the center of mass of ^{12}C cluster. A similar situation with two configurations in the ground state is found for ^{6}He, ^{6}Li [2–4, 7] or ^{10}Be, ^{10}C [5, 6] nuclei, where the center of mass of the dinucleon subsystem coincides (one configuration) or does not coincide (another configuration) with the center of mass of the subsystem of α-particles.

VII. MOMENTUM DISTRIBUTIONS

To complete the study of the structure functions of ^{14}C and ^{14}O nuclei, we present the momentum distributions of α-particles and extra nucleons in these systems within the five-particle model.

The momentum distribution $n_i(k)$ of the i-th particle is known to be the density of the probability to find this particle with a definite momentum k,

$$n_i(k) = \left\langle \tilde{\Phi} \right| \delta\left(\mathbf{k} - (\mathbf{k}_i - \mathbf{K}_{c.m.})\right) \left| \tilde{\Phi} \right\rangle, \tag{18}$$

where $\tilde{\Phi}$ is the wave function of the system in the momentum representation. The normalization of the momentum distribution is $\int n_i(k)\, d\mathbf{k} = 1$. The momentum distribution $n_i(k)$ enables one, in particular, to calculate the average kinetic energy of the i-th particle:

$$\langle E_{i,kin} \rangle = \int \frac{k^2}{2m_i} n_i(k)\, d\mathbf{k}. \tag{19}$$

Mainly due to the mass ratio between a nucleon and an α-particle, the extra nucleons move much more rapidly than the α-particles inside ^{14}C and ^{14}O nuclei. In particular, the calculated kinetic energy of each of the extra neutrons in ^{14}C nucleus is about 32.66 MeV, while the same value for an α-particle amounts about 6.83 MeV. For ^{14}O nucleus, we have 31.77 MeV for an extra proton, and 6.62 MeV for an α-particle. The corresponding ratio of velocities is about 4.4 (for both nuclei). This means that the extra nucleons move essentially faster than the heavier α-particles do.

The momentum distributions are very close for both considered nuclei. That is why, we present the profiles of the momentum distributions only for ^{14}C. In Fig. 7, curve 1 corresponds to the momentum distribution of an α-particle, and curve 2 depicts $n_n(k)$ of an extra neutron. The momentum distribution of α-particles $n_\alpha(k)$ is seen to be a monotonically decreasing function, while $n_n(k)$ has two maxima: at zero momentum and at $k^2 \simeq 1$ fm^{-2}. These two maxima correspond to two above-mentioned configurations in the ground state of the nucleus. In a configuration, where an extra neutron is comparatively far from the center of the nucleus, it moves comparatively slowly and makes a contribution to the peak at very small k^2. As for configurations, where the extra neutrons move mainly inside ^{12}C cluster, their momenta are somewhat greater, and they make their contribution to the second maximum at $k^2 \simeq 1$ fm^{-2}. At the same time, the α-particles inside ^{12}C cluster almost do not feel the extra neutrons motion peculiarities, and, thus, their influence on the momentum distribution of α-particles is small due to the mass ratio and the comparatively large binding energy of ^{12}C cluster.

VIII. CONCLUSIONS

To sum up, we note that the mirror nuclei ^{14}C and ^{14}O have very close structures of their ground-state wave functions, ^{14}O nucleus having a little bit greater size and a less binding energy because of the additional Coulomb repulsion due to the charges of extra protons. At the same time, it is shown that the r.m.s. charge radius of ^{14}O nucleus is less than that of ^{14}C due to the position of extra nucleons mainly inside ^{12}C cluster. The r.m.s. charge radius of ^{14}O nucleus is predicted. The charge density distribution and the elastic charge form factor of ^{14}C nucleus are shown to be essentially different from the same values for ^{14}O, whereas the distributions independent of the charges of particles are almost coincide (including probability density distributions of particles, pair correlation functions, and the momentum distributions). Two configurations in the ground-state wave function are revealed, where ^{12}C cluster and the dinucleon subsystem have the same centers of mass (first configuration, with a dinucleon inside ^{12}C cluster), or shifted centers of mass (second configuration, with one nucleon outside of ^{12}C cluster).

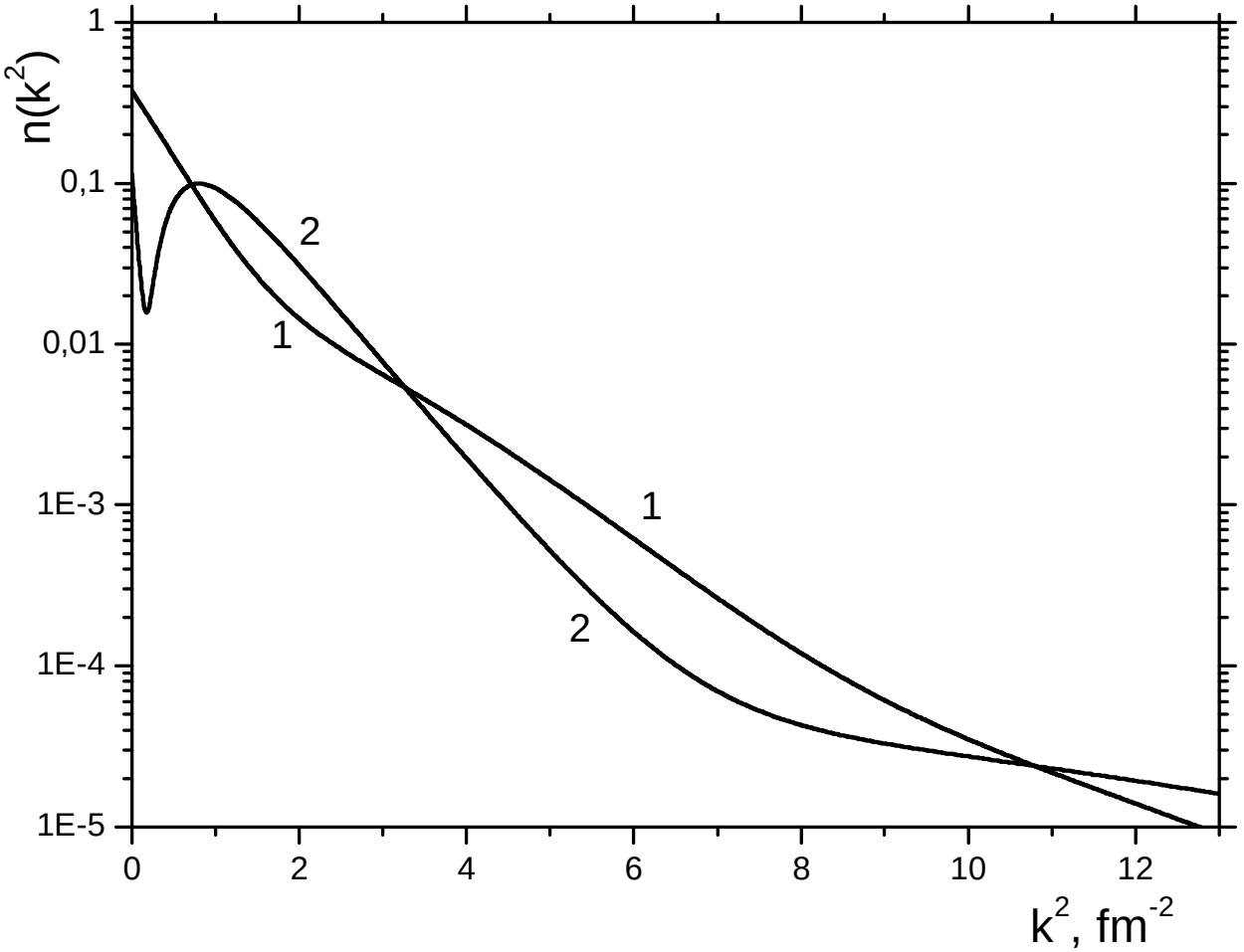

Figure 7: Momentum distributions of an α-particle (curve 1) and an extra neutron (curve 2) in ^{14}C nucleus

Acknowledgment

This work was supported in part by the Program of Fundamental Research of the Department of Physics and Astronomy of the National Academy of Sciences of Ukraine (project No. 0112U000056).

[1] B. E. Grinyuk, D. V. Piatnytskyi, Ukr. J. Phys. **61**, 674 (2016) doi:10.15407/ujpe61.08.0674

[2] V. I. Kukulin, V. N. Pomerantsev, Kh. D. Razikov, V. T. Voronchev, G. G. Ryzhikh, Nucl. Phys. **A 586**, 151 (1995) doi:10.1016/0375-9474(94)00494-8

[3] M. V. Zhukov, B. V. Danilin, D. V. Fedorov, J. M. Bang, I. J. Thompson, J. S. Vaagen, Phys. Reports **231**, 151 (1993) doi:10.1016/0370-1573(93)90141-Y

[4] B. E. Grinyuk, I. V. Simenog, Physics of Atomic Nuclei **72**, 6 (2009) doi:10.1134/S1063778809010025

[5] Y. Ogawa, K. Arai, Y. Suzuki, K. Varga, Nucl. Phys. **A 673**, 122 (2000) doi:10.1016/S0375-9474(00)00133-0

[6] B. E. Grinyuk, I. V. Simenog, Physics of Atomic Nuclei **77**, 415 (2014) doi:10.1134/S1063778814030090

[7] A. V. Nesterov, F. Arickx, J. Broeckhove, V. S. Vasilevsky, Phys. Part. Nucl. **41**, 716 (2010) doi:10.1134/S1063779610050047

[8] V. I. Kukulin, V. M. Krasnopol'sky, J. Phys. G: Nucl. Phys. **3**, 795 (1977) doi:10.1088/0305-4616/3/6/011

[9] Y. Suzuki, K. Varga, *Stochastic Variational Approach to Quantum-Mechanical Few-Body Problems* (Springer, Berlin, 1998) doi:10.1007/3-540-49541-X

[10] V. G. Neudatchin, V. I. Kukulin, V. L. Korotkikh, V. P. Korennoy, Phys. Lett. **B 34**, 581 (1971) doi:10.1016/0370-2693(71)90142-0.

[11] V. I. Kukulin, V. G. Neudatchin, Yu. F. Smirnov, Fiz. Élem. Chastits At. Yadra **10**, 1236 (1979) (Sov. J. Part. Nucl. **10**, 492 (1979))

[12] R. H. Helm, Phys. Rev. **104**, 1466 (1956) doi:10.1103/PhysRev.104.1466

[13] A. I. Akhiezer, V. B. Berestetskii, *Quantum Electrodynamics* (Interscience, New York, 1965)

[14] R. F. Frosch, J. S. McCarthy, R. E. Rand, M. R. Yearian, Phys. Rev. **160**, 874 (1967) doi:10.1103/PhysRev.160.874

[15] I. Angeli, K. P. Marinova, Atomic Data and Nuclear Data Tables **99**, 69 (2013) doi:10.1016/j.adt.2011.12.006

[16] I. Sick, Phys. Rev. C **77**, 041302(R) (2008) doi:10.1103/PhysRevC.77.041302

[17] H. Crannell, Phys. Rev. **148**, 1107 (1966) doi:10.1103/PhysRev.148.1107

[18] I. Sick, J. S. McCarthy, Nucl. Phys. **A150**, 631 (1970) doi:10.1016/0375-9474(70)90423-9

[19] P. E. Bosted *et al.*, Phys. Rev. Lett. **68**, 3841 (1992) doi:10.1103/PhysRevLett.68.3841